Three dimensional finite element study of the behaviour and failure mechanism of non-crimp fabric composites under in-plane compression

Authors: Luis Miguel Ferreira[1] (corresponding author), Enrique Graciani, Federico París

Affiliation (All Authors): Grupo de Elasticidad y Resistencia de Materiales, Escuela Técnica Superior de Ingenieros, Universidad de Sevilla.
Address:
Grupo de Elasticidad y Resistencia de Materiales.
Escuela Técnica Superior de Ingenieros.
Camino de los Descubrimientos s/n.
41092 Sevilla, España
Phone: (+34) 954 487 300
Fax: (+34) 954 461 637
Email: lferreira@hct.ac.ae (Luis Miguel Ferreira), egraciani@us.es (Enrique Graciani), fparis@us.es (Federico París).

Abstract
The compressive behaviour and the mechanism responsible for failure of a $[0,90]_n$ non-crimp fabric (NCF) laminate are studied using a 3D finite element (FE) model of the representative unit cell at the mesoscopic scale. The tows of the unit cell were generated using a straight FE mesh taking into account the waviness of the fibres with the definition of the mechanical properties of each element according to the actual direction of the fibres. A parametric study has been carried out to evaluate the influence of the non-linear behaviour of the tows and of the fibre crimp on the compressive failure mechanism of the laminate. The numerical predictions are discussed and compared with experimental data. The results lead to think that the mechanism of failure of a $[0,90]_n$ NCF laminate under a pure compressive load is controlled by the shear strains that appear in the crimp part of the 0º tows. It is also found that the non-linear behaviour of the tows and the fibre crimp substantially contribute to the development of the potential failure initiation mechanism. A satisfactory agreement between the numerical and experimental compressive stress-strain curves is obtained for the highest fibre crimp angles considered.
Keywords

---

[1] Higher Colleges of Technology, Abu Dhabi Men's College
P.O. Box 25035, Abu Dhabi, United Arab Emirates

Composites; Non-crimp fabric (NCF); Finite element model (FEM); Compressive behaviour; Failure Mechanism.

1. Introduction

The need to combine the excellent in-plane behaviour of the composites made from unidirectional layers of pre-impregnated tapes (UDPT) with the lower cost and better out-of-plane behaviour of the woven fabric composites led to the appearance of the non-crimp fabric (NCF) composites [1]. These composites are made from dry preforms which are produced in a continuous process by sequentially laying groups of fibre tows, or tows for short, at a specific orientation, sequentially on a conveyor system. Once the tows are laid at all the orientations required, they are held in position by a stitching yarn creating, in theory, a fabric without fibre crimp. In practice, however, some geometrical features are introduced at the manufacturing stage of the preforms and others later on at the moulding stage, such as resin pockets between the tows and some mesoscopic fibre crimp, (Fig. 1 [2]); the latter has particular interest for this study since it is strongly related to the compressive performance of NCF composites [3-5].

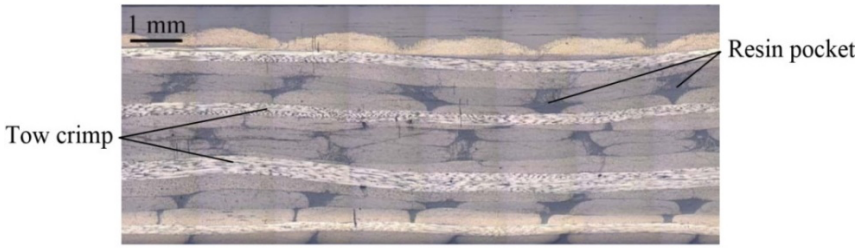

Fig. 1. Cross-section of a typical NCF composite.

Due to the complex internal structure of the NCF composites, performing representative studies using Finite Element (FE) models becomes a complicated task. Some representative studies have been performed using a 2D approach [3, 6, 7]. However, the complex mesoscopic architecture of these materials may not be completely represented by a 2D FE model [5], since it is highly irregular along all directions of the material. Moreover, this approach does not allow the stresses and strains at the 3D mesomechanical level to be calculated. These limitations motivated the development of parametric mesoscopic 3D FE models capable of reproducing the complex 3D structure of a NCF laminate.

The study presented in this paper, of the compressive behaviour and failure mechanism of NCF composites, has been achieved using 3D FE models of the representative unit cell of a $[0,90]_n$ NCF laminate, represented in Section 2.1. The stiffness properties of the constituents and the boundary conditions imposed are described in Sections 2.2 and 2.3, respectively. The compressive behaviour results, which are presented in Section 3, emphasize the shear stresses/strains components associated with the mechanism of failure and how the non-linear behaviour of the tows and the fibre crimp affect the compressive performance of the NCF laminate. In Section 4, the numerical predictions are discussed

and compared with the experimental evidence obtained from the work carried out on the FALCOM Project (Failure Performance and Processing Prediction for Enhanced Design with Non-Crimp Fabric Composites). The numerical analysis has been carried out using a FE model with straight mesh, following the modelling approach presented in [8]. In Section 5, the results obtained with the FE models with a straight mesh are compared with those obtained with the *Classical Modelling Approach* (using a curved mesh) to show the better performance of the FE models with a straight mesh. Finally, the conclusions are set out in Section 6.

2. Mesoscopic approach of the NCF laminate

Before presenting the mesoscopic scale 3D FE models developed for this study, it is necessary to define the concept of the representative unit cell (RUC): a repeatable cell which allows any part of the NCF laminate to be generated just by assembling multiple RUC's. This concept is illustrated in Fig. 2 using a $[0,90]_2$ NCF laminate.

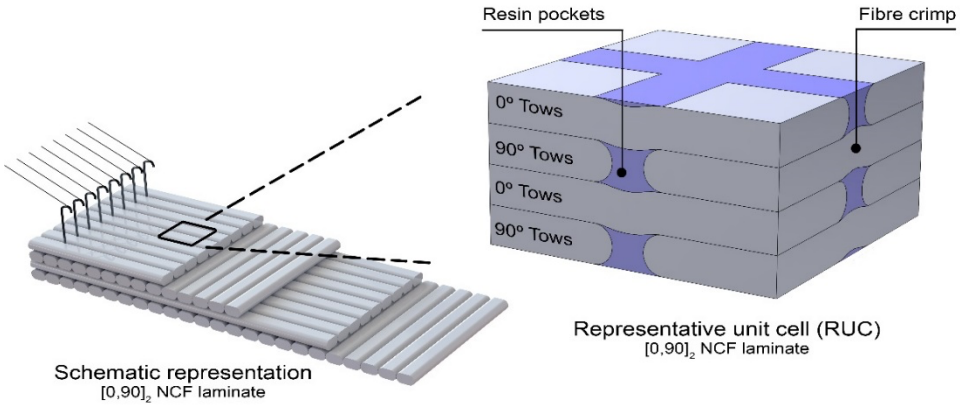

Fig. 2. Process used to obtain the representative unit cell of a $[0,90]_2$ NCF laminate.

At the mesoscopic level, an NCF laminate can be thought of as a stack of layers of fibre tows (in different orientations) with homogeneous transversely isotropic behaviour, the isotropic plane normal to the fibres being surrounded by an homogeneous isotropic matrix.

2.1. Numerical models

A mesoscopic scale 3D FE model of the RUC of a $[0,90]_n$ NCF laminate with fibre crimp, due to nesting of the tows, was generated using structural solid element SOLID45 from ANSYS® FE code [9]. The unit cell is composed of 4 laminas (0º, 90º, 0º, 90º) and each lamina contains two half-tows with a resin pocket between them, see Fig. 3(a) and Fig. 3(b). Notice that the resin has been removed to better understand the tows' shape and orientation. Some of the geometrical parameters, which appear in Fig. 3, will be defined later.

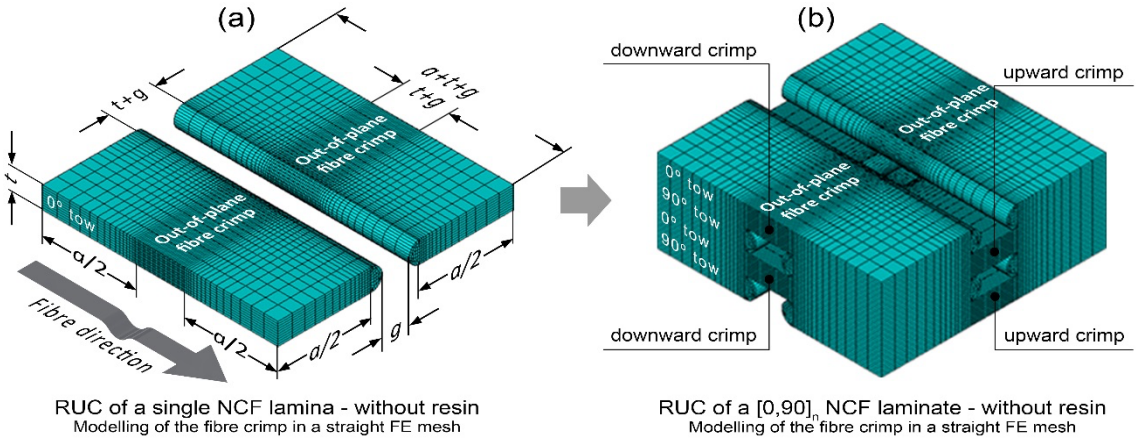

Fig. 3. 3D FE model of the representative unit cell without resin.
(a) Single NCF lamina, (b) $[0,90]_n$ NCF laminate.

The curvature of the tows has not been included in the geometry of the model, however the waviness of the fibres has been taken into consideration, see Fig. 4(a), following the modelling approach presented in [8]. This approach obviously allows a straight FE mesh, as represented in Fig. 4(b), to be used. An isolated element with the appropriate orientation of the fibres in shown in Fig. 4(c). Notice that α is the angle between the fibre direction 1 and the ideal longitudinal direction of the tow (x in the 0º tows and y in the 90º tows) and will be referred to as the *misorientation angle* from now on. β is an angular parameter that corresponds to the maximum misorientation angle and thus represents the maximum fibre crimp of the tow, that is: $\beta = \max(\alpha)$.

A maximum fibre crimp angle of 9º was chosen for the initial studies, based on the fact that previous results showed a satisfactory agreement between the apparent in-plane stiffness properties and the experimental evidence for angles in the range of 9º to 12º [4, 10]. In what follows, the fibre crimp was parametrically varied (in a range of 0º to 12º) in order to reveal the influence of this geometrical heterogeneity over the compressive behaviour and failure mechanism of $[0,90]_n$ NCF laminates.

The geometrical parameters employed are shown in Fig. 3(a), where a represents the length of the tow not affected by the fibre crimp, t the thickness of each lamina and g the width of the gap between two adjacent tows for each lamina. The values of these parameters have been estimated from the results of the microstructure characterization measured in [11] having taken, $a = 2.06$ mm, $t = 0.24$ mm and $g = 0.30$ mm. The value of these parameters and the maximum fibre crimp angle are identical for all the tows. An average fibre volume fraction for each lamina of $V_f^l = 60\%$ has been obtained from the observed average fibre volume fraction of the tows $V_f^t = 69\%$ [12] and the relative dimensions of the cross-sections of the tow and of the lamina.

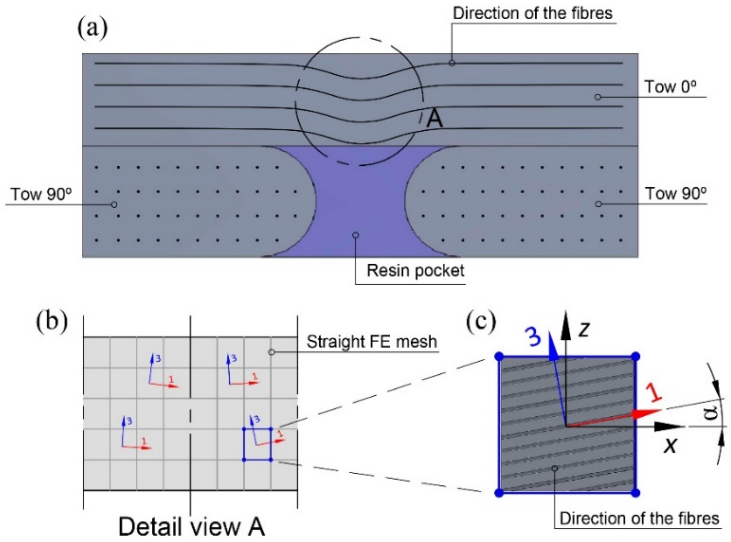

Fig. 4. Schematic representation of the approach used for modelling the waviness of the fibres in 3D FE models [8]: (a) NCF composite with fibre crimp, (b) detailed view of the FE mesh in the fibre crimped area, (c) isolated straight element.

Taking advantage of the symmetry of the problem to improve the computing efficiency, only one quarter of the RUC has been employed in this study, see Fig. 5. In accordance with the global coordinate system *xyz* represented in Fig. 5, the plane of the laminate is the *xy*-plane and *z* is the through-thickness direction. The local coordinate system 123 corresponds to the actual direction of the fibres.

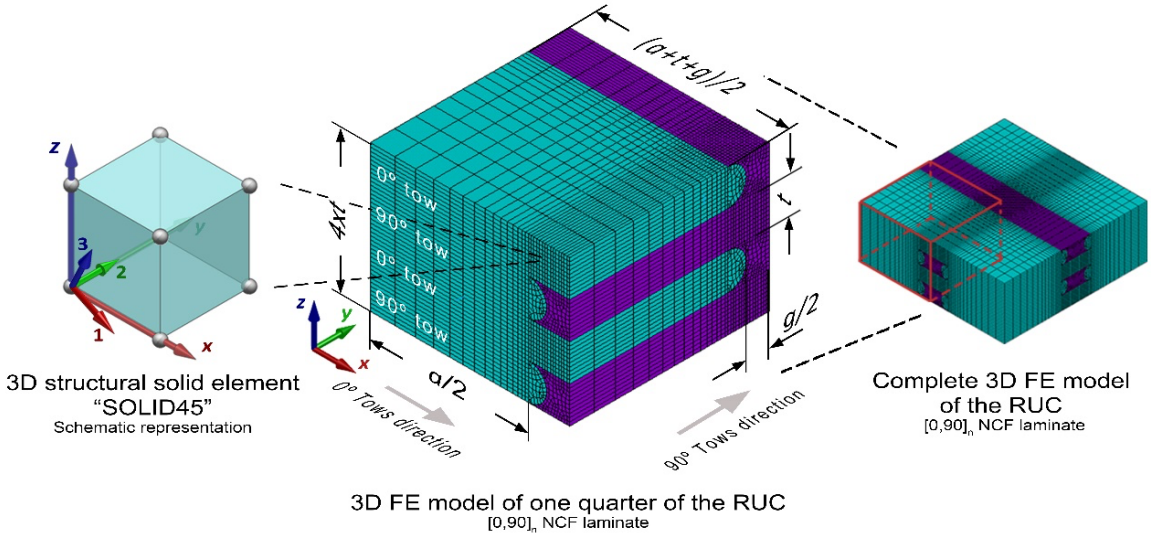

Fig. 5. 3D FE model and dimensions of a quarter of the $[0,90]_n$ NCF laminate developed.

Different mesh discretizations were used in the study to assess its influence on the results. The use of coarser meshes led to the appearance of intermittent evolutions of stresses and strains along the part where the tows present the fibre crimp. As there are no stress

intensification factors, the mesh was progressively refined until these evolutions became smoother. As it is possible to appreciate in Fig. 5, particular attention was given to crimped part of the tows where a finer mesh was employed. This area corresponds to a potential failure initiation location when looking for a mechanism of failure.

2.2. Mechanical properties of the constituents

At the mesoscopic scale, the stiffness properties required in order to carry out the FE analysis are those of the resin pockets and of the tows. Since the tows are constituted by a large number of parallel fibres, uniformly distributed and impregnated by a resin, their behaviour can be considered transversely isotropic (with elastic constants: $E_{11}^t,\ \nu_{12}^t, G_{12}^t, E_{22}^t,\ \nu_{23}^t$ and G_{23}^t).

The FE model has been generated according to the NCF composites tested within the FALCOM Project [13-15]. However, as no experimental measurements were performed to estimate the stiffness properties of the tows, the rule of mixtures has been employed as an averaging technique to estimate their values as a function of the elastic properties of the fibre and of the resin, see Table 1.

V_f^t	$E_{11}^t\,(\mathrm{GPa})$	$E_{22}^t\,(\mathrm{GPa})$	ν_{12}^t	ν_{23}^t	$G_{12}^t\,(\mathrm{GPa})$	$G_{23}^t\,(\mathrm{GPa})$
60%	165.5	11.43	0.30	0.42	4.03	4.03

Table 1. Stiffness properties of the tows obtained using the rule of mixtures.

The resin employed has the following elastic properties: an elastic modulus $E^m = 3.50\,\mathrm{GPa}$, a Poisson's ratio $\nu^m = 0.42$ and a corresponding shear modulus $G^m = 1.23$ GPa. Carbon fibres, being a transversely isotropic material, exhibit the following relationships: $E_{22}^f = E_{33}^f,\ \nu_{12}^f = \nu_{13}^f,\ G_{12}^f = G_{13}^f$. According to the rule of mixtures, the values of the elastic constants $\left(E_{22}^f,\ \nu_{23}^f \text{ and } G_{23}^f\right)$, in the planes transverse to the fibre axis, are not required to estimate the apparent stiffness properties of the tows neither in the longitudinal plane nor in the transverse planes. Therefore, the carbon fibre has been characterized by a longitudinal elastic modulus $E_{11}^f = 237\,\mathrm{GPa}$, a Poisson's ratio $\nu_{12}^f = 0.25$ and a shear modulus $G_{12}^f = 94.8\,\mathrm{GPa}$.

The tows were modelled with linear shear behaviour in the transverse plane (23-plane) and with non-linear shear behaviour in the longitudinal and transverse through-thickness planes (12-plane and 13-plane, respectively), because in these latter planes the behaviour of the tows under shear loads is affected by the resin, whose behaviour is also non-linear [3]. This non-linearity in the mechanical behaviour of the tows was introduced into the FE model by a bilinear approximation of the shear stress-strain curve obtained by Ditcher [16]. The change of slope was defined to occur at a value $\left(\sigma_{12}^*\right)$ of 60 MPa of stress and 1.4% of strain, see Table 2.

$\sigma_{12}^{*}\,(\mathrm{MPa})$	Slope I $G_{12}^{t,I}=G_{13}^{t,I}\,(\mathrm{GPa})$	Slope II $G_{12}^{t,II}=G_{13}^{t,II}\,(\mathrm{GPa})$
60	4.03	0.75

Table 2. σ_{12}^{*}, slope values I and II used to define the non-linear shear behaviour of the tows.

Several studies were also performed in order to assess the influence of the behaviour of the neat resin within the resin pockets (linear elastic and non-linear elastic) on the compressive response of the NCF laminate. No significant changes in the results were appreciated. Therefore, in order to facilitate the convergence of the solutions, the behaviour of the resin within the resin pockets has been defined as linear.

2.3. Boundary conditions

The boundary conditions applied to the faces of the model, see Table 3, serve to impose a compressive stress state and to guarantee the displacements compatibility between the limits of the model and the rest of the structure. With reference to the global coordinate system *xyz*, represented in Fig. 5, symmetry conditions have been assumed in the faces parallel to the *xz*-plane and one of the faces parallel to the *yz*-plane. On the opposite face, parallel to the *yz*-plane, a constant displacement *(k)* in the compression load direction has been applied to all nodes, and to ensure that they all displace the same, all nodes have been coupled. The compression load, therefore, is the result of the sum of the reaction forces of all nodes at $x=0$. The boundary conditions on the top and bottom faces (parallel to the *xy*-plane) must guarantee the compatibility of the unit cell under consideration with the adjacent unit cells. Thus, the displacements of the nodes on both faces are coupled to ensure that the extension in the through-thickness direction is constant throughout the whole model. Notice that with the boundary conditions employed, the NCF laminate has an infinite length along the *y*-axis.

Model faces	Boundary conditions	Schematic representation
$x=0$	$u_x=k,\ k>0 \mid \sigma_{xy}=0 \mid \sigma_{xz}=0$	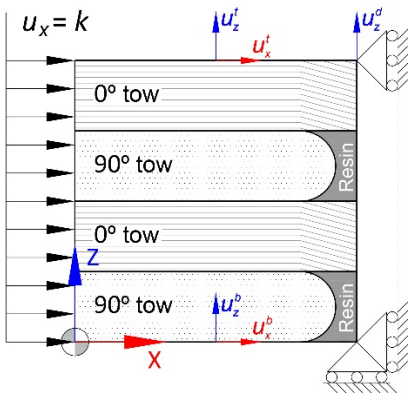
$x=\dfrac{(a+t+g)}{2}$	$u_x=0 \mid \sigma_{xy}=0 \mid \sigma_{xz}=0$	
$y=0$	$u_y=0 \mid \sigma_{xy}=0 \mid \sigma_{yz}=0$	
$y=\dfrac{(a+t+g)}{2}$	$u_y=0 \mid \sigma_{xy}=0 \mid \sigma_{yz}=0$	
$z=0 \mid z=4t$	$u_x^t=u_x^b \mid u_y^t=u_y^b \mid u_z^t-u_z^b=u_z^d$	

Table 3. Boundary conditions imposed.

3. Compressive behaviour and failure mechanism

This section focuses on studying the compressive behaviour and failure mechanism of a $[0,90]_n$ NCF laminate by means of FE analysis. The study was performed with the command option NLGEOM, ON [9], so that it includes large displacements, large rotations and large strain effects. The equilibrium is satisfied in the deformed shape and the load is applied in a linear and progressive form until instability occurs.

It is clear that, due to the boundary conditions and to the load imposed, the normal stress component in the 0º tows will present larger values than any other stress component in any other part of the unit cell (90º tows or resin). However, given the presence of the fibre crimp, it is expected that the 0º tows will suffer a shear instability phenomenon, known as *mesobuckling*, that causes localized shear strains [3, 5]. In the present study (and with reference to the aforementioned), the evolutions of these shear strains and shear stresses stood out when looking for a mechanism of failure.

3.1. Stresses and strains in the potential failure location

Since the fibre crimp has been modelled in the through-thickness direction, the most relevant shear stress/strain components to be analysed when looking for the mechanism of failure are σ_{xz} and γ_{xz} (results expressed in the global axis of the problem). The distribution of σ_{xz} and γ_{xz} throughout the unit cell with $\beta = 9^{\circ}$ for a compressive load of 0.5 GPa, can be observed in Fig. 6(a) and Fig. 6(b), respectively. Note that Fig. 6 displays the solution results as continuous contours across element boundaries for the selected nodes and elements. These contours are determined by linear interpolations within each element from the nodal values, which are averaged at a node whenever two or more elements connect to the same node.

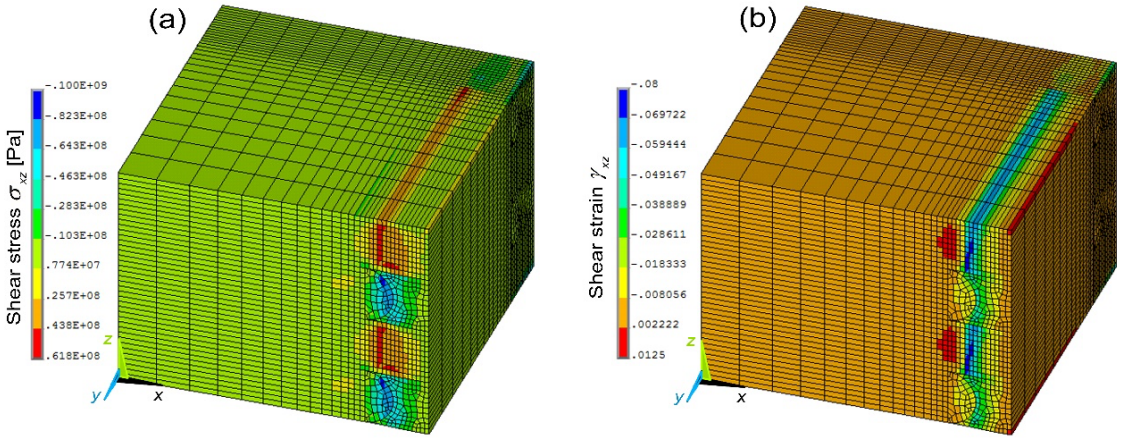

Fig. 6. Numerical results throughout the unit cell for a compressive load of 0.5GPa. (a) Shear stresses σ_{xz} (b) Shear strains γ_{xz}.

It can be observed that in the left-hand part of the figures, where there are neither matrix elements nor fibre crimp, no significant changes in σ_{xz} and γ_{xz} appear. The greatest stress and strain gradients arise in the part where the 0º tows are affected by the fibre crimp and

where the packages of resin appear between each pair of 90º tows. The results also show that both highly positive and highly negative shear strains are placed very close together and are located at the part of the 0º tow where the misorientation angle is greatest. This mechanism can be clearly observed in Fig. 7 where detailed views of the undeformed and deformed shapes are represented in the area where the fibres are crimped. The same scale has been employed for both figures.

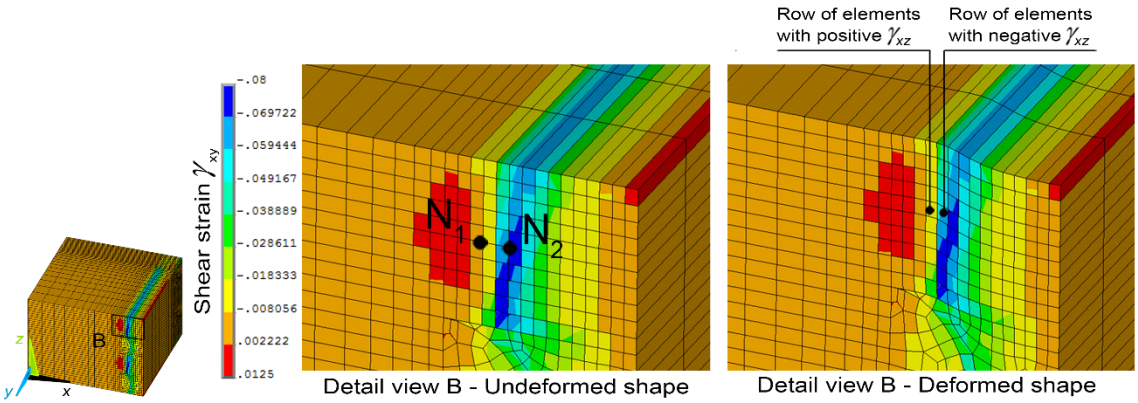

Fig. 7. Undeformed and deformed shapes in the area under analysis with location of nodes N_1 and N_2.

It is also possible to appreciate the distribution of shear strain along two consecutive vertical rows of elements in the 0º tows, one of them with a positive value of γ_{xz} and the other with a negative value of γ_{xz} (greater in absolute value than the previous one). This evolution of γ_{xz} throughout the *xy*-plane along the actual direction of the fibres in the middle of a 0º tow, is shown in Fig. 8 as direction *A*. Notice that several levels of the applied compressive load are represented and that "Load 100%" corresponds to the load at which the numerical solution stops converging (0.58 GPa). For load values higher than "Load 100%", the elements in the crimped area of the 0º tows (aligned with the load direction), with higher values of α, became exceedingly distorted and the solution was unable to converge. Notice that the load at which the solution stops converging has nothing to do with the failure of the laminate, rather it depends on a great number of parameters, such as the quality of the mesh, the element type, time control of the solution and the selected equation solver.

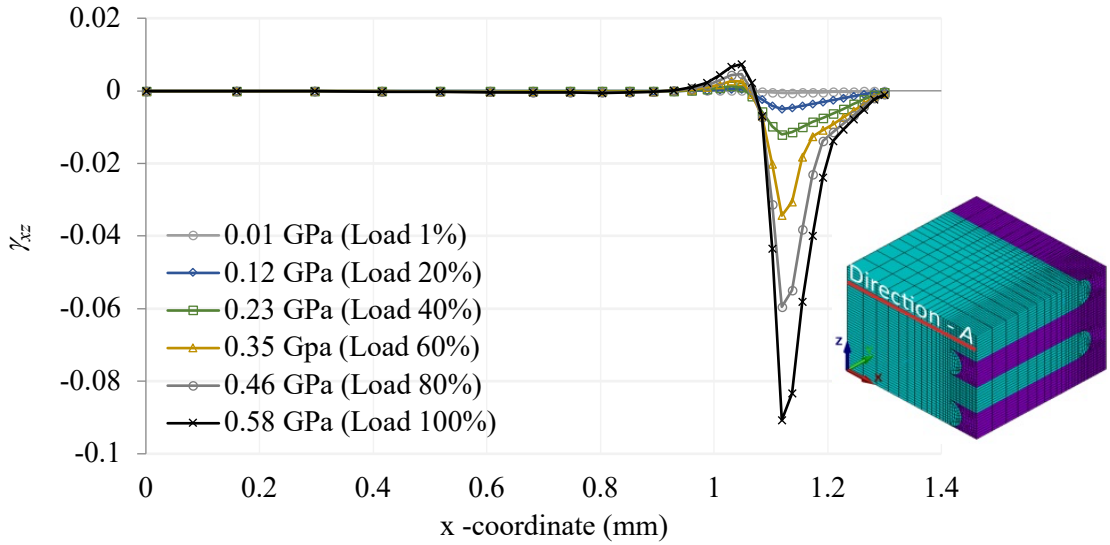

Fig. 8. Evolution of γ_{xz} at the *xy*-plane along direction *A* for several levels of the applied load.

This behaviour of γ_{xz} has been confirmed to be generalized along direction *y*, thus making it reasonable to surmise that it could be a potential location for failure initiation.
In order to understand how the fibre crimp of the tows (oriented in the same direction of the applied load) and how their mechanical behaviour might affect this potential mechanism of failure, a parametric study was performed. The results obtained are presented in Sections 3.2 and 3.3, respectively.

3.2. Influence of the non-linear behaviour of the tows

To understand how the non-linear shear behaviour of the tows affects the compressive behaviour of a $[0,90]_n$ NCF laminate, the results obtained for a unit cell with $\beta = 9^o$ (in the following "*nonlinear material model"*) were compared with the results obtained with an identical unit cell in which the tows were modelled as an orthotropic linear elastic material (in the following "*linear material model*"). A comparison was made between the γ_{xz} of nodes N_1 and N_2, see Fig. 7, and the applied compressive load until the solution stops converging, see Fig. 9.

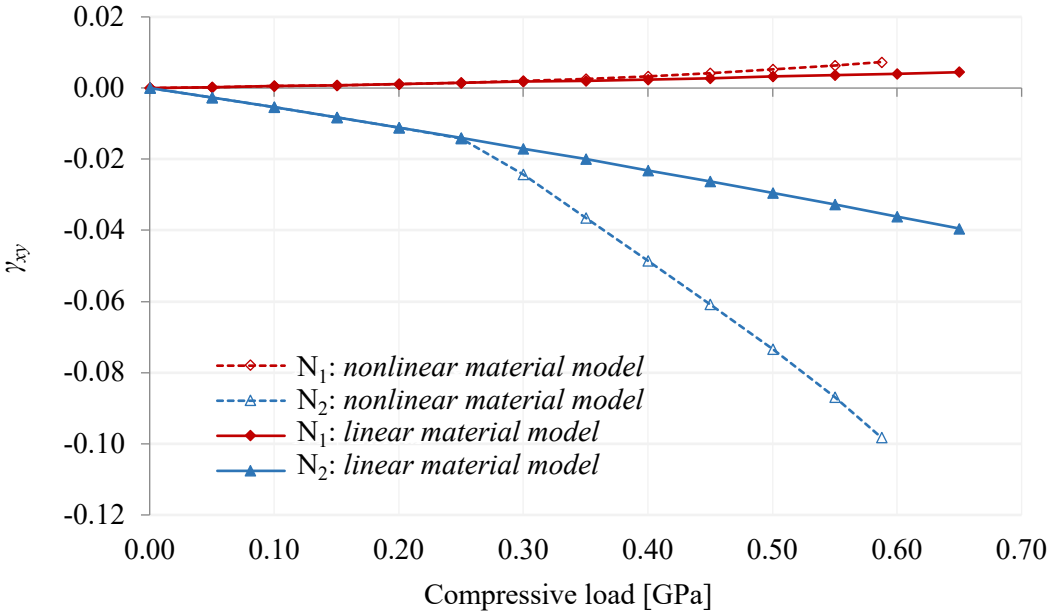

Fig. 9. Evolution of γ_{xy} with the applied compressive load for both models considered.

The results show that for small compressive loads the linear and non-linear curves are identical, however, from approximately 0.25 GPa, (load at which certain elements of the *nonlinear material model* reach the second part of the bilinear shear constitutive equation of the tows) the *nonlinear material model* curves change their slope and significant differences appear between the two models. This change in the non-linear curves is more evident in the negative shear strains. It can be seen that the maximum jump of γ_{xy} in the *linear material model* is from +0.45% to -3.95%, while for the *nonlinear material model* it is from +0.73% to -9.83%, which corresponds to an increase of 140%.

The non-linear shear behaviour of the tows clearly influences the elastic solution associated to the aforementioned potential failure mechanism and, consequently, it has to be considered in future studies if quantitative failure loads are going to be determined.

3.3. Influence of the fibre crimp of the tows

As has been analysed in section 3.1, the mechanism responsible for failure of a NCF laminate is closely linked to the presence of the fibre crimp in the tows, which are oriented along the same direction of the applied load. Moreover, it has been deduced that the mechanism of failure may be associated with the jump in γ_{xz}. Therefore, an increase in the value of the fibre crimp angle is expected to increase the shear stress/strain gradients in the crimped part of the 0º tows. To confirm this behaviour, the evolution of σ_{xz} and γ_{xz} at the *xz*-plane along direction *A* was obtained for fibre crimp angles in a range of 3º to 12º and for a compressive load of 0.5 GPa.

The results show that both σ_{xz} and γ_{xz} develop smoothly when the fibres are straight independently of the fibre crimp angle considered, see Fig. 10 and Fig. 11, respectively.

However, this behaviour is abruptly interrupted when the fibres start to crimp (i.e, where packages of resin appear between the 90º tows) and localized high shear stresses/strains arise. As expected, higher fibre crimp angles lead to higher absolute values of σ_{xz} and γ_{xz}.

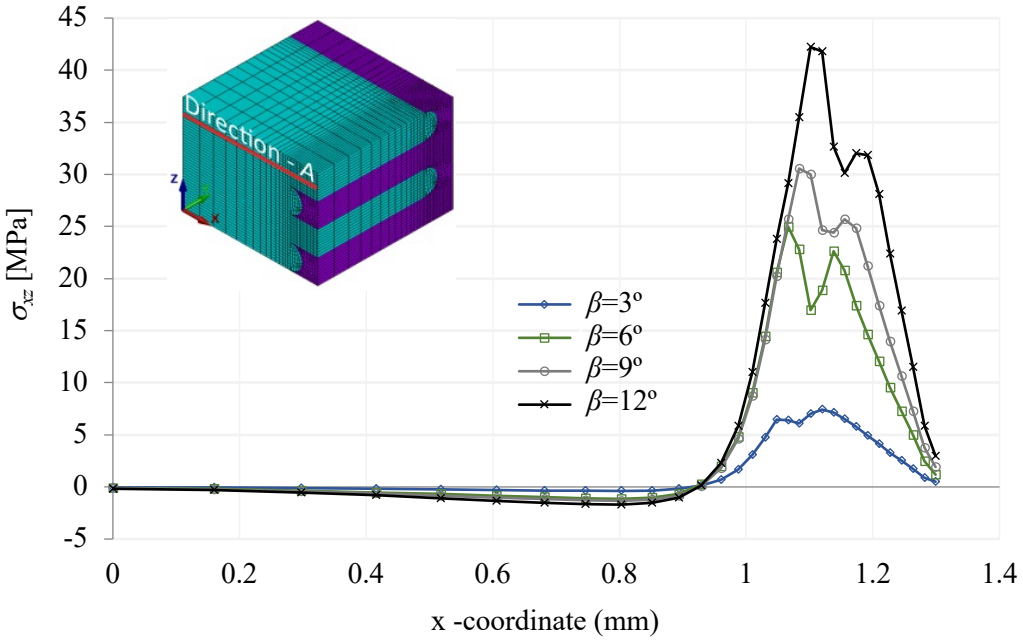

Fig. 10. Influence of the variation of the fibre crimp on the behaviour of σ_{xz} along direction A for a compressive load of 0.5 GPa.

A slight negative slope of σ_{xz} along the straight part of the tows can be observed in Fig. 10, however, very close to the part where the fibres start to crimp, σ_{xz} inverts its slope and starts to increase exponentially until it reaches an apex near the elements with the highest misorientation angle. The subsequent decrease of σ_{xz} is explained by the reduction of the misorientation angle of the elements that model the fibre crimp, with the value of σ_{xz} always remaining positive. The trough observed for all values of β, between the two relative maximum values, is due to the tridimensional interaction in the anisotropic constitutive law on the *xy*-plane. Notice that the associated shear strain γ_{xz}, see Fig. 11, has a continuous evolution along Direction *A*.

The evolution of γ_{xz} along direction *A* presented in Fig. 11, shows that due to the absence of matrix elements under the straight part of the tows, no significant changes in γ_{xz} appear. However, as for σ_{xz}, an abrupt change in the behaviour occurs when the fibres start to crimp. The results show that positive and high negative shear strains are both placed very close to each other and that the jump starts to take place at a location where the 0º tows stop being in contact with the adjacent 90º tows and begin to be in contact

with the resin. The negative values increase until they reach their maximum in the elements with the highest misorientation angle. The change of slope in the negative values of γ_{xz}, for the unit cells with $\beta \geq 6^{o}$, is associated with the fact that the shear stress-strain behaviour of the tows has been defined by a bilinear evolution.

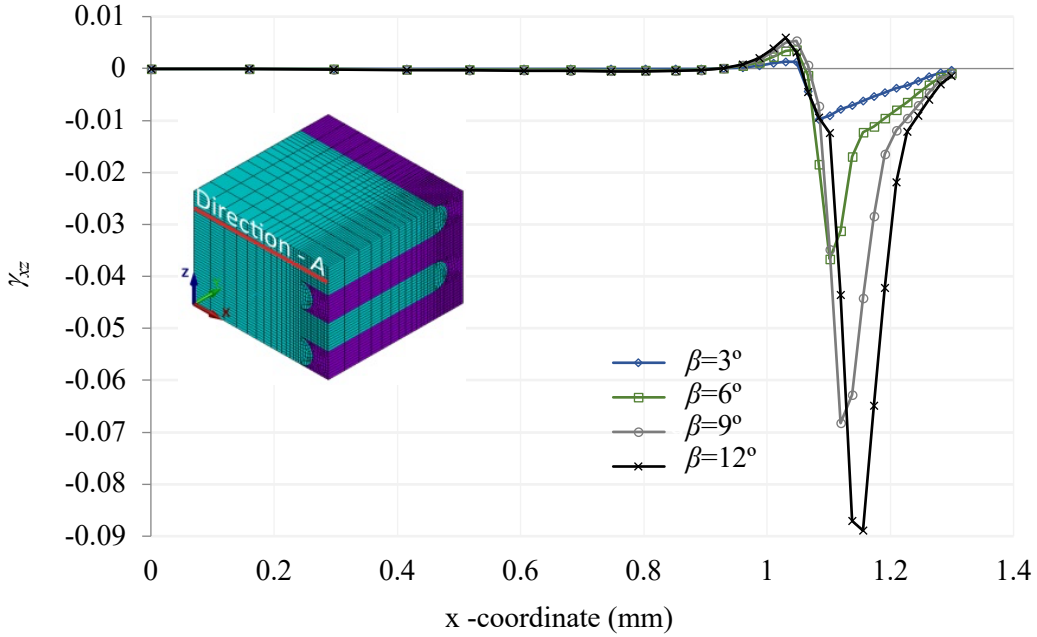

Fig. 11. Influence of the variation of the fibre crimp on the behaviour of γ_{xz} along direction *A* for a compressive load of 0.5 GPa.

It can also be observed, that the increase in the fibre crimp angle causes a slight separation between the points defining the aforementioned jump (those with maximum and minimum values of γ_{xz}); this happens because the maximum misorientation angle changes its position in the tow towards the crimp axis when the fibre crimp angle increases.

The results also show that when the maximum fibre crimp increases from 3º to 12º, σ_{xz} increases from a maximum value of 7.5 MPa to 41.8 MPa (an increase of 457%) and γ_{xz} increases from a maximum value of -0.94% to -8.89% (an increase of 845%). Therefore, it can be concluded that the localized shear stresses/strains are strongly dependent on the fibre crimp angle.

Notice that the significant differences between the evolution of the shear stress and shear strain curves in the part of the tow where the fibres are crimped, is explained by the fact that the rotation of the stress tensor to express the results in the global coordinate system causes the elements with negative γ_{xz} to have positive σ_{xz}.

Having identified the potential location and the mechanism responsible for the compressive failure of the NCF laminate, the numerical results are compared with experimental data in the following section.

4. Comparison with the experimental results

To validate the results obtained with the 3D FE model of the RUC of a $[0,90]_n$ NCF laminate, the numerical compressive stress-strain curves for several fibre crimp angles, in a range of 0º to 18º, were compared with the experimental data obtained from the FALCOM Project [17], see Fig. 12.

The numerically predicted compressive stress-strain curves show a non-linear behaviour, this non-linear behaviour being more noticeable when the fibre crimp angle increases.

As can be appreciated in Fig. 12, the higher the value of the fibre crimp angle, the lower the compressive load at which the numerical solution stops converging. This is mainly due to the fact that elements become highly distorted for lower loads when higher fibre crimp angles are employed. This distortion can be easily observed in Fig. 9, where for a compressive load of 0.58 GPa the shear strain γ_{xy} is nearly 9%.

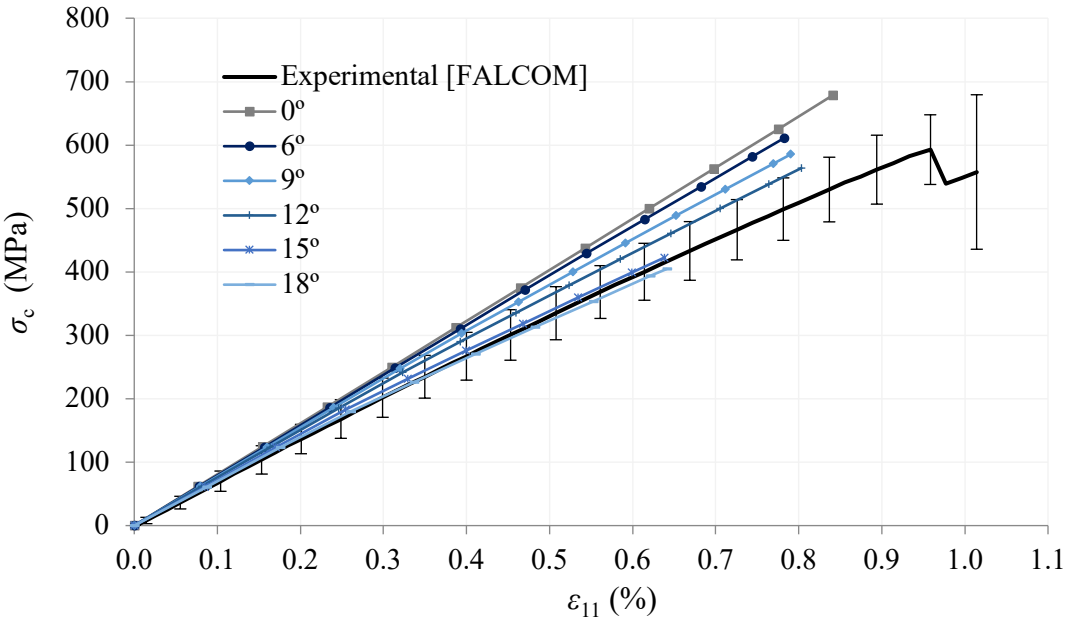

Fig. 12. Numerical results obtained for a fibre crimp angles in a range of 0º to 18º and experimental data.

A satisfactory agreement with the experimental stress-strain curve is found for fibre crimp angles between 12º to 18º. Although the averaged value of the fibre crimp angle that affects the tows of the specimens was not characterized, these results are in line with [8], where the numerically obtained in-plane stiffness properties for a fibre crimp angle of 12º are in agreement with the experimental averaged stiffness properties of the specimens.

The numerical solution that best adjust to the mean value of all tested specimens [17] is obtained for a fibre crimp angle of 15º that includes the non-linear behaviour of the tows. However this solution stops converging at a strain of 0.64% while the experimental data indicates that failure occurs at approximately 1%. Since convergence for higher strains has not been achieved it is not possible to assess if the solution will continue adjusting or if it will diverge when the accumulation of damage starts to affect the global behaviour of the specimens.

These issues have started to be object of analysis in [18] where the material property degradation of the tows has been included in the simulations. Despite of the fact ANSYS® only allows the progressive damage analysis to be performed in linear elastic materials, a satisfactory agreement with experimental data, in terms of curve fitting and failure load, has been obtained. Additionally, the results confirm that damage initiates in the part where the 0º tows are affected by the fibre crimp which corresponds to the potential location of the failure mechanism identified in this paper.

5. Validation of the modelling approach

To ensure the validity of the modelling approach, the numerical results obtained within the considered range of fibre crimp angles, were compared with equivalent RUC's in which the fibre crimp was modelled according to the *Classical Modelling Approach* (CMA) [8], see Fig. 13.

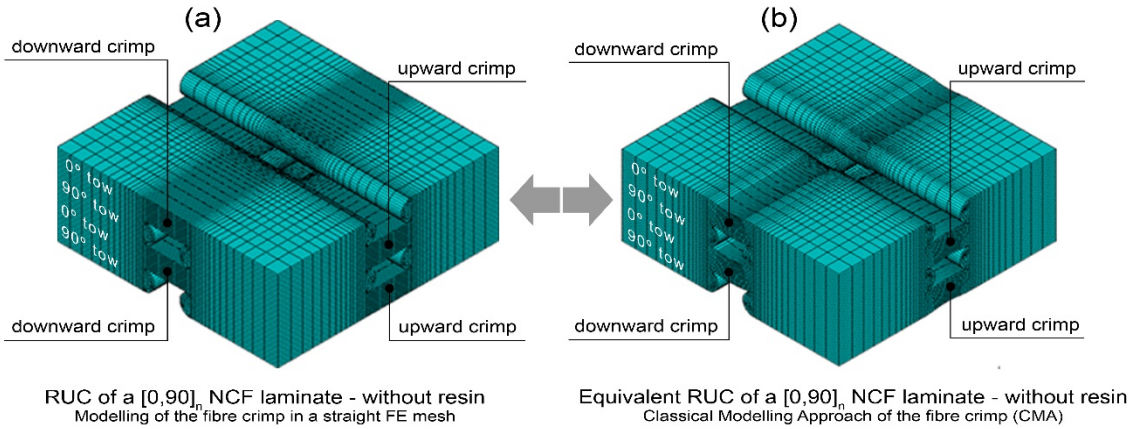

Fig. 13. Comparison between modelling approaches of the fibre crimp. (a) Modelling with a Straight FE Mesh. (b) Classical Modelling Approach.

Similar solutions were obtained with both methods which confirms the fact that the approach employed for modelling the fibre crimp is a valid alternative when generating 3D FE models of NCF composites with fibre crimped tows. Furthermore, it has been found that the CMA presents more convergence issues in the non-linear analyses than the straight FE mesh method. These convergence issues appeared in the straight FE mesh solutions at about 170% of the load in which they appeared in the CMA solutions,

independently of the crimp angle considered. These evidences can be appreciated in Fig. 14, where the numerical results for both methods (for fibre crimp angles of 9º and 15º) and the experimental data are presented.

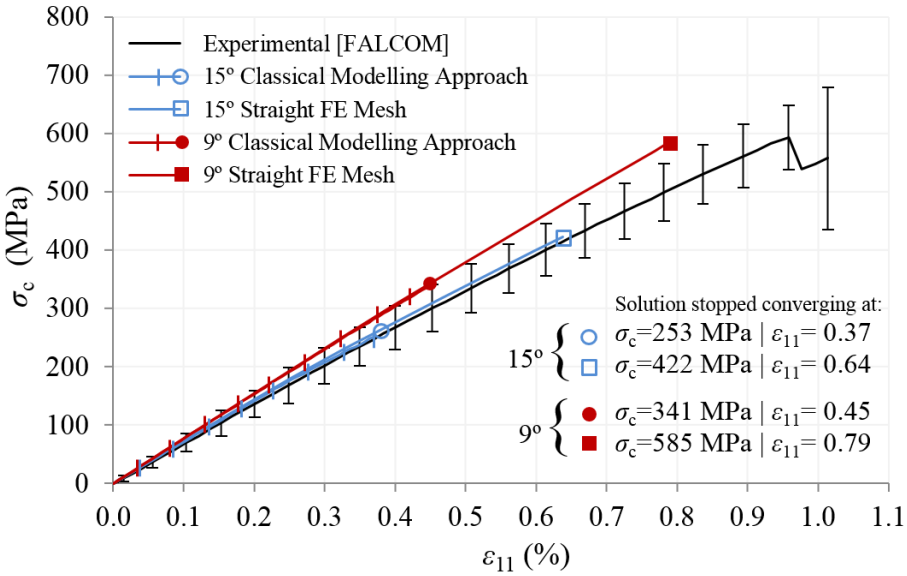

Fig. 14. Numerical results obtained with RUC's with the fibre crimp modelled with the *Classical Modelling Approach* and with a *Straight FE Mesh* and the experimental data.

Apart from the observable influence of the fibre crimp angle on the convergence of the solution, several studies have also been performed to analyse how parameters, such as: the FE mesh discretization (coarser and finer 3D FE meshes); the element type (SOLID45 and SOLID185); the time control of the solution (different time step sizes) and the selected equation solver (sparse direct, pre-condition CG), could affect the convergence [9]. It has been found that the load at which the numerical solution stops converging, for any of the fibre crimp angles employed, is strongly dependant on these parameters. The results presented were obtain after a process of optimization of the aforementioned parameters so that the lack of convergence of the solution occurred at the highest load possible.

6. Conclusions

The behaviour of a $[0,90]_n$ NCF laminate under an in-plane compressive load has been studied using 3D FE models with fibre crimped tows. It can be observed from the results that the potential mechanism of failure of a $[0,90]_n$ NCF laminate that has been identified under this type of load is controlled by the shear strains that appear in the crimp part of the 0º tows. Maximum positive and maximum negative shear strains, on the *xz*-plane, are seen to be located very close together, in the area where the 0º tow stops being in contact with the adjacent 90º tow and reaches the maximum misorientation angle. These results are in agreement with studies, using a 2D approach, which were performed to investigate

the compressive strength of NCF laminates. However, this 2D approach did not allow the stresses and strains at the 3D mesomechanical level to be calculated. This limitation motivated the development of the parametric 3D FE models capable of reproducing the complex 3D mesoscopic structure of a NCF laminate.

The influence of the non-linear shear behaviour of the tows on the compressive failure mechanism has also been analysed. The results show that including the non-linear behaviour in the tows causes an increase in the shear stresses/strains particularly in the crimped area of the 0º tows (aligned with the load direction) hence contributing to the development of the potential failure mechanism. It has also been demonstrated that the size of the jump of the shear strains is directly related to the fibre crimp angle: the higher the fibre crimp angles, the higher the shear strains.

To validate the results obtained with the unit cell, the numerically predicted compressive stress-strain curves were compared with the experimental measurements carried out on the FALCOM Project. A fairly good prediction of the numerical compressive stress-strain curve for the NCF laminate has been obtained for fibre crimp angles in a range of 12º to 18º. In particular, the solution that best adjusted to the mean value of all tested specimens was obtained with a 15º but convergence issues appeared for lower strains. In this way, it is not possible to verify if the solution would continue adjusting for higher strains when the accumulation of damage started to affect the global behaviour of the specimens nor it is possible predict failure.

To validate the straight FE mesh modelling approach the results were compared with the results obtained with equivalent RUC's in which the fibre crimp was modelled according to the *Classical Modelling Approach*. Similar solutions were obtained with both methods but the *Classical Modelling Approach* presented more convergence issues in the non-linear analyses than the straight FE mesh approach.

The parametric 3D models of the RUC of a $[0,90]_n$ NCF laminate that have been generated were employed in a progressive damage analysis [18] and a satisfactory agreement with experimental data has been obtained. Additionally, the results confirmed that damage initiates in the part where the 0º tows are affected by the fibre crimp which corresponds to the potential location of the failure mechanism identified in this paper.

Bibliography

[1] Bibo GA, Hogg PJ, Kemp M. Mechanical characterisation of glass- and carbon-fibre-reinforced composites made with non-crimp fabrics. Composites Science and Technology. 1997;57:1221-41.

[2] Mattsson D, Joffe R, Varna J. Methodology for characterization of internal structure parameters governing performance in NCF composites. Composites Part B-Engineering. 2007;38:44-57.

[3] Drapier S, Wisnom MR. Finite-element investigation of the compressive strength of non-crimp-fabric-based composites. Composites Science and Technology. 1999;59:1287-97.

[4] Ferreira LM. Study of the behaviour of non-crimp fabric laminates by 3D finite element models. PhD. Thesis. Sevilla: University of Seville, 2012.
[5] París F, González A, Graciani E, Flores M, Castillo E. A 3D FEM study of compressive behaviour of non-crimp fabrics, (paper FM7). In Proceedings: 11th European Conference on Composite Materials (ECCM11). Rhodes, Greece 2004.
[6] Drapier S, Wisnom MR. A finite-element investigation of the interlaminar shear behaviour of non-crimp-fabric-based composites. Composites Science and Technology. 1999;59:2351-62.
[7] Joffe R, Mattsson D, Modniks J, Varna J. Compressive failure analysis of non-crimp fabric composites with large out-of-plane misalignment of fiber bundles. Composites Part a-Applied Science and Manufacturing. 2005;36:1030-46.
[8] Ferreira LM, Graciani E, París F. Modelling the waviness of the fibres in non-crimp fabric composites using 3D finite element models with straight tows. Composite Structures. 2014;107:79-87.
[9] ANSYS. Release 15. Swanson Analysis Systems Inc 2014.
[10] González A, Graciani E, París F. Prediction of in-plane stiffness properties of non-crimp fabric laminates by means of 3D finite element analysis. Composites Science and Technology. 2008;68:121-31.
[11] Mattsson D, Joffe R, Varna J. Characterisation of processability and manufacturing. Characterisation of microstructure. FALCOM/WP2:D2.1-4/LTU. 2004.
[12] Asp LE, Öhgren I, Holmberg JA. Determination of fibre content on RFI plates for G1c and OHT testing. FALCOM/WP3/SI/TECH001. 2004.
[13] Joffe R. Characterization of performance. Performance in tension. Elastic properties and failure. FALCOM/WP3:T3.2.1/LTU. 2004.
[14] Joffe R. Performance of non-crimp fabric composites in shear. Trends in Composite Materials and Their Design. 2010;425:45-59.
[15] Mattsson D, Joffe R, Varna J. Damage in NCF composites under tension: Effect of layer stacking sequence. Engineering Fracture Mechanics. 2008;75:2666-82.
[16] Ditcher AK. The non-linear stress-strain behaviour of carbon fibre reinforced plastic and its effects on the analysis of laminated plates and sandwich beams. Bristol, UK: University of Bristol, 1981.
[17] Sinclar R, Robinson P, Iannucci L. Directed compression tests on FALCOM biaxial cross-ply material. FALCOM/WP3/ICL/TR01. Imperial College London; 2005.
[18] Ferreira LM, Graciani E, París F. Progressive damage study of NCF composites under compressive loading. 16th European Conference on Composite Materials, ECCM 2014: European Conference on Composite Materials, ECCM; 2014.